REPORT DOCUMENTATION PAGE

Form Approved
OMB No. 0704-0188

1. REPORT DATE *(DD-MM-YYYY)*	2. REPORT TYPE	3. DATES COVERED *(From - To)*
	Technical Papers	

4. TITLE AND SUBTITLE

5a. CONTRACT NUMBER N/A

5b. GRANT NUMBER

5c. PROGRAM ELEMENT NUMBER

6. AUTHOR(S)

5d. PROJECT NUMBER 2308

5e. TASK NUMBER M19B

5f. WORK UNIT NUMBER

7. PERFORMING ORGANIZATION NAME(S) AND ADDRESS(ES)

Air Force Research Laboratory (AFMC)
AFRL/PRS
5 Pollux Drive
Edwards AFB CA 93524-7048

8. PERFORMING ORGANIZATION REPORT

9. SPONSORING / MONITORING AGENCY NAME(S) AND ADDRESS(ES)

Air Force Research Laboratory (AFMC)
AFRL/PRS
5 Pollux Drive
Edwards AFB CA 93524-7048

10. SPONSOR/MONITOR'S ACRONYM(S)

11. SPONSOR/MONITOR'S NUMBER(S)

12. DISTRIBUTION / AVAILABILITY STATEMENT

Approved for public release; distribution unlimited.

13. SUPPLEMENTARY NOTES

14. ABSTRACT

15. SUBJECT TERMS

16. SECURITY CLASSIFICATION OF:			17. LIMITATION OF ABSTRACT	18. NUMBER OF PAGES	19a. NAME OF RESPONSIBLE PERSON
a. REPORT	b. ABSTRACT	c. THIS PAGE			Leilani Richardson
Unclassified	Unclassified	Unclassified	A		19b. TELEPHONE NUMBER *(include area code)* (661) 275-5015

Standard Form 298 (Rev. 8-98)
Prescribed by ANSI Std. 239.18

21 separate items enclosed

23 08 M19B

MEMORANDUM FOR PRS (Contractor/In-House Publication)

FROM: PROI (TI) (STINFO) 25 Oct 2000

SUBJECT: Authorization for Release of Technical Information, Control Number: **AFRL-PR-ED-AB-2000-208**
Vaghjiana, Ghanshyam (ERC), "Kinetics of OH Reactions with N_2H_4, CH_3NHNH_2 and $(CH_3)_2NNH_2$ in the Gas Phase"

International Journal of Chemical Kinetics **(Statement A)**
(Deadline: 30 Sep 2000 – PAST DUE)

1. This request has been reviewed by the Foreign Disclosure Office for: a.) appropriateness of distribution statement, b.) military/national critical technology, c.) export controls or distribution restrictions, d.) appropriateness for release to a foreign nation, and e.) technical sensitivity and/or economic sensitivity.
Comments:_____

Signature _____ Date _____

2. This request has been reviewed by the Public Affairs Office for: a.) appropriateness for public release and/or b) possible higher headquarters review
Comments: _____

Signature _____ Date _____

3. This request has been reviewed by the STINFO for: a.) changes if approved as amended, b.) appropriateness of distribution statement, c.) military/national critical technology, d.) economic sensitivity, e.) parallel review completed if required, and f.) format and completion of meeting clearance form if required
Comments:_____

Signature _____ Date _____

4. This request has been reviewed by PRS for: a.) technical accuracy, b.) appropriateness for audience, c.) appropriateness of distribution statement, d.) technical sensitivity and economic sensitivity, e.) military/ national critical technology, and f.) data rights and patentability
Comments:_____

APPROVED/APPROVED AS AMENDED/DISAPPROVED

_____
PHILIP A. KESSEL Date
Technical Advisor

Cleared (PA)_____
Logged (PA)_____
Notified (PA)_____
Copied & Distributed (STINFO)_____
This original is for PA files

Kinetics of OH Reactions With N_2H_4, CH_3NHNH_2 and $(CH_3)_2NNH_2$ in the Gas Phase

GHANSHYAM L. VAGHJIANI

ERC
Air Force Research Laboratory
AFRL/PRSA
10 E Saturn Blvd
Edwards AFB, CA 93524
Tel: 661 275 5657
Fax: 661 275 6245
Email: ghanshyam.vaghjiani@ple.af.mil

ABSTRACT

The gas phase reaction kinetics of OH with three di-amine rocket fuels; N_2H_4, CH_3NHNH_2 and $(CH_3)_2NNH_2$ was studied in a discharge flow-tube apparatus and a pulsed-photolysis reactor under pseudo-first-order conditions in [OH]. Direct laser-induced fluorescence monitoring of the [OH] temporal profiles in a known excess of the [di-amine] yielded the following absolute second-order OH rate coefficient expressions; $k_1 = (2.17 \pm 0.39) \times 10^{-11} e^{(160 \pm 30)/T}$, $k_2 = (4.59 \pm 0.83) \times 10^{-11} e^{(85 \pm 35)/T}$ and $k_3 = (3.35 \pm 0.60) \times 10^{-11} e^{(175 \pm 25)/T}$ cm^3 $molec^{-1}$ s^{-1}, respectively, for reactions with N_2H_4, CH_3NHNH_2 and $(CH_3)_2NNH_2$ in the temperature range 232-637 K. All three reactions did not show any discernable pressure dependence on He or N_2 buffer gas pressure of up to 530 torr. The magnitude, and the weak temperature and the lack of pressure effects of the OH + N_2H_4 reaction

rate coefficient suggests that a simple direct metathesis of H-atom may not be important compared to addition of the OH to one of the N-centers of the di-amine skeleton, followed by rapid dissociation of the intermediate into products. Our findings on this reaction are qualitatively consistent with a previous ab-initio study [*Armstrong et al. J Phys Chem A 1997, 101, 4761*]. However, in the alkylated di-amines, direct H-abstraction from the methyl moiety can not be completely ruled out.

INTRODUCTION

Hydrazine (N_2H_4), methylhydrazine (CH_3NHNH_2) and unsymmetrical dimethylhydrazine ($(CH_3)_2NNH_2$) form an important class of di-amine based rocket fuels. Understanding the reactivity of OH radicals towards these di-amines is important in accurately modeling the combustion of these fuels with nitrogen tetroxide, and for assessing their environmental human health impact when inadvertently released into the lower atmosphere near launch pads. The other tropospheric oxidant for these fuels is expected to be ozone. To our knowledge, no accurate reaction rate coefficient data is available in the literature for the O_3 reactions, and only two groups **[1,2]** have reported a limited data set on the rate coefficient, k_1 for the OH + N_2H_4 reaction. The 298 K values of k_1 differ by a factor of ~ 3 in these two studies. A brief study on the rate coefficient, k_2 for the OH + CH_3NHNH_2 reaction has also been carried out previously **[1]**. There is no data to be found on the direct measurement of the rate coefficient, k_3 for the OH + $(CH_3)_2NNH_2$ reaction.

Here we report a detailed study of the gas phase kinetics of OH reactions with the three di-amines in the temperature range 232-637 K and for He or N_2 buffer gas pressure of up to 530 torr. The experimental observations are discussed in terms of a reaction mechanism involving the initial addition of the OH to the di-amine molecule followed by rapid dissociation of the intermediate to products [3].

EXPERIMENTAL TECHNIQUE

Previously, we have described the details of the fast flow-tube apparatus and the pulsed-photoylsis reactor **[4,5]**. Here, we only give the details of reagent preparations, and how the reaction kinetics data were collected and analyzed.

The di-amine plus OH reactions were studied under pseudo-first-order conditions in OH concentration ([OH] << [di-amine]). The gas phase [di-amine] concentration in the experiments was determined by uv photometric techniques, and accurate measurements of the system's pressure, temperature and carrier gas flow rates using previously calibrated capacitance manometers, thermocouples and electronic mass-flow meters. The uv-absorption cross sections, $\sigma_{213.9\text{-nm}}$ of 220.5 x 10^{-20}, 248.9 x 10^{-20} and 399.9 x 10^{-20} cm^2 $molec^{-1}$, respectively for N_2H_4, CH_3NHNH_2 and $(CH_3)_2NNH_2$ were used **[4,6]**. The Teflon/Pyrex flow-lines were previously conditioned with the di-amines so that its in-situ decomposition in the reactors was negligible. The OH was probed using a tunable pulsed-laser operating at ~ 282.15 nm to excite the Q_12 line of the OH transition, ($A^2\Sigma^+$, $v' = 1 \leftarrow X^2\Pi$, $v'' = 0$). The resulting laser-induced

fluorescence due to the transitions, ($A^2\Sigma^+$, v' = 1 $\rightarrow$ $X^2\Pi$, v" = 1, bandhead at 312.16 nm) and ($A^2\Sigma^+$, v' = 0 $\rightarrow$ $X^2\Pi$, v" = 0, bandhead at 306.36 nm), ensuing from the detection zone was detected orthogonally to the probe laser beam by gated-charge integration/signal averaging techniques **[5,7]**.

The OH was generated either in a fixed side-arm or in a sliding double-injector microwave discharge port of the fast flow-tube apparatus. The inside walls of the port were coated with a 30% solution of H_3PO_4 acid to minimize loss of the precursor radicals for OH production. 1% H_2 in He or 1% CF_4 in He mixtures were discharged to produce H-atoms and F-atoms, respectively. These were immediately titrated downstream of the plasma with NO_2 and H_2O, respectively, to produce OH radicals before injecting them into a known amount of the di-amine being carried by He with a total linear bulk-flow velocity, v. (The di-amine entered the main reaction zone of the flow-tube from the sliding injector when the OH was produced in the side-arm, and vice versa.) All surfaces that came in contact with the OH were coated with a halocarbon wax to reduce the loss rate of OH to the walls. The flow-tube was operated under plug-flow conditions at a nominal He pressure of ~ 2 torr and in the temperature range 232-374 K. Below 232 K, the loss rate of OH to the walls in the presence of the di-amine was so high that the signal-to-noise ratio of the OH-fluorescence fell below the detection limit (of 1 x 10^9 molec cm^{-3} per 1000-pulse-integrations). The flow-tube had to be warmed to 232 K or above in order to recover the OH signal to its original level. Similarly above 374 K, the OH could not be detected, this time due to fogging of the cooler optical components of the detection chamber from condensation of the halocarbon wax vapor ensuing from the heated reaction zone of the flow-tube. At each [di-amine], the kinetics of the OH plus di-amine reaction was followed by

recording the steady-state OH-fluorescence signal strength as a function of the reaction distance, z between the point of reagent mixing at the injector tip and the fixed detection zone downstream of the flow-tube.

A pulsed-photolysis reactor operating at up to 530 torr of He pressure under slow-flow conditions was employed to extend the rate coefficient measurements to 637 K. Data at higher temperatures was not collected as significant charring of the inside surfaces of the reactor was observed due to heterogeneous decomposition of the alkylated di-amines. A premixed flow of N_2O, and H_2O and di-amine vapors in He was subjected to 193-nm laser photolysis to generate the hydroxyl radicals ($N_2O + h\nu \rightarrow N_2 + O(^1D)$ followed by $O(^1D) + H_2O \rightarrow 2OH$ **[8,9]**). In this setup, the kinetics was followed by determining the [OH] time profile immediately after the photolysis by recording the relative OH-fluorescence signal strength as a function of the delay time between the photolysis and probe laser pulses.

Materials

He (>99.9997%) from U. S. Bureau of Mines, N_2 (99.9995%) from Spectra Gases and N_2O (99.99%) from Matheson Gas Products were used as received. Hydrocarbon-free N_2H_4 (Viking Grade) from Edwards AFB, $(CH_3)_2NNH_2$ (>99.3%) and CH_3NHNH_2 (>99.5%) from Olin Chemicals were subjected to several freeze-thaw purification cycles at a grease-less vacuum line, and the purified distillates dried over BaO or CaH_2. NO_2 (99.9%) from M. G. Scientific Gases was mixed with excess O_2 to react away any NO present and the mixture collected in a

trap over silica gel at 213 K. The excess O_2 and any other volatiles were pumped off and the condensate subjected to several freeze-thaw purification cycles. A standard 1% NO_2 in He titration mixture was prepared. O_2 (99.991%) from Big Three Industries, CF_4 (99.7%) from Scott Specialty and H_2 (99.999%) from Linde Specialty Gases were used as supplied to make up a 1% in He discharge mixtures. The water was distilled in the laboratory.

RESULTS

Since the [di-amine] is always in a great excess over the [OH] in the flow-tube, it can be shown that the pseudo-first-order decay coefficient, k, for OH radicals is given by, $\ln\{OHS/OHS_o\} = -k.t.$ Where OHS is the net (background-subtracted) steady-state OH-fluorescence signal strength recorded at the detection zone for a reaction time of $t = z/v$. The flow-tube reaction distance, z, is defined to be the length between the tip of the injector where the OH enters and the OH-fluorescence detection axis. v is the bulk linear flow velocity of the He carrier gas. OHS_o is the net signal strength that would be observed for $z = 0$ and corresponds to the initial concentration, $[OH]_o$ available at the detection zone. $k = k_W + k_i[\text{di-amine}]$, where k_W is the first-order loss rate term for OH radicals to the walls, and k_i the absolute second-order OH reaction rate coefficient with the di-amine ($i = 1$, 2, or 3 for N_2H_4, CH_3NHNH_2 and $(CH_3)_2NNH_2$, respectively). Values of k in the range 100-600 s^{-1} were extracted from non-linear-least-squares fits to the data points of the observed exponential decays of the OH radical signal, see Figure 1. In the absence of the di-amine, k_W was typically found to

be ~ 30-40 s^{-1} at 298 K. (For OH entering upstream via the fixed side-arm port, there is additional loss of OH, that increases as the reaction length is decreased due to increasing amount of exposure to the injector walls. This lost rate term, $k_{w,i}$ was typically found to be ~ 10 s^{-1} at 298 K.) The values of k were plotted as a function of [di-amine] to extract the corresponding k_i values by fitting the data to a linear-least-squares routine, see Figure 2.

In the pulsed-photolysis experiments, the OH signal after the initiating laser pulse is recorded as a function of the delay time between the photolysis and probe laser pulses. Again, exponential profiles were recorded with decay coefficients, k given by; $k_d + k_1$[di-amine]. Here, k_d represents the sum of first-order loss rate terms of OH due to diffusion out of the detection volume and reaction with background impurities. k_d was typically measured to be in the range 50-100 s^{-1} and k in the range 500-5000 s^{-1}.

Tables I, II and III show the values of k_i determined in this work with the experimental conditions employed. Variation in the initial hydroxyl radical concentration, $[OH]_o$ employed or the source chemistry utilized had no systematic effect on the k_i values, showing that the influence of any source radicals or secondary OH reactions on the rate coefficient determinations is negligible. Also, no discernable pressure effect of k_i was observed in this work for up to 530 torr of He. k_1 was also found to be independent of N_2 pressure of up to 403 torr. Data in N_2 was obtained by looking at the temporal profile of the hydroxyl radical in the reaction of O-atoms with N_2H_4 which is known to yield OH(v") **[5]**. O-atoms were produced by the rapid N_2 quenching of $O(^1D)$ generated in the 193-nm photolysis of N_2O **[10]**. Sufficient CO_2 is added

to the photolysis mixture, such that it preferentially quenches the OH(v") product to its ground v" = 0 state before any significant reactive loss takes place [11]. The observed OH-fluorescence profiles were fitted to a bi-exponential expression as described previously [5] to extract the absolute second-order reaction rate coefficients, $k_{1(phenomenological)}$ and k_O, respectively, for OH and O-atom [12] reactions with hydrazine, see Figure 3. The temperature dependencies of k_i are summarized in Figure 4.

DISCUSSION

The reactions of OH with the di-amines are very fast, close to the gas-kinetic limit, and show slight negative temperature dependencies. The Arrhenius fits to the data points of Figure 4 give the following expressions; $k_1 = (2.17 \pm 0.39) \times 10^{-11} e^{(160 \pm 30)/T}$, $k_2 = (4.59 \pm 0.83) \times 10^{-11} e^{(85 \pm 35)/T}$ and $k_3 = (3.35 \pm 0.60) \times 10^{-11} e^{(175 \pm 25)/T}$ cm^3 $molec^{-1}$ s^{-1}, respectively, for reactions with N_2H_4, CH_3NHNH_2 and $(CH_3)_2NNH_2$ in the temperature range 232-637 K, and for employed He or N_2 pressure of up to 530 torr. Previous flash photolysis-resonance fluorescence study of Harris et al. [1] reported a temperature dependence of $4.4 \times 10^{-11} e^{(116 \pm 176)/T}$ cm^3 $molec^{-1}$ s^{-1}, in the range 298-424 K, for the OH + N_2H_4 reaction. No dependence was observed on the Ar pressure used which was varied in the range 25-50 torr. Also under their conditions, a temperature independent rate coefficient of $(6.5 \pm 1.3) \times 10^{-11}$ cm^3 $molec^{-1}$ s^{-1} was reported for the OH + CH_3NHNH_2 reaction. However, for the OH + $(CH_3)_2NNH_2$ reaction, they could only estimate a room temperature value of $(5 \pm 2) \times 10^{-11}$ cm^3 $molec^{-1}$ s^{-1}

because of severe handling problems encountered with this dialkylated di-amine. At 298 K, Harris et al.'s values are ~ 75% larger, ~ 6% larger and ~ 17% smaller than our values for N_2H_4, CH_3NHNH_2 and $(CH_3)_2NNH_2$, respectively. An earlier communication from Hack et al. [2] for the OH + N_2H_4 reaction studied by discharge flow-tube-ESR technique reported a value of 2.2×10^{-11} cm^3 $molec^{-1}$ s^{-1} at 298 K which is ~ 41% smaller than our value. Harris et al.'s values for the alkylated di-amines are in very good agreement with the present study. However, their absolute N_2H_4 values differ significantly from ours, though the reported temperature dependence agrees reasonably well. The lack of proper quantification of the N_2H_4 number density in their and Hack et al.'s work might possibly be one of the reasons as to why there is disagreement in the absolute values for k_1. We have made accurate, to within ± ~ 6% [6], in-situ measurements of the [di-amine] in our experiments and have confirmed that the measured rate coefficients are independent of the $[OH]_o$ range employed. The overall accuracy of the rate coefficients in this work is calculated to be ~ ± 18% (1-σ precision plus systematic errors) [5]. Some problematic wall effects were noticed when using $(CH_3)_2NNH_2$, especially at temperatures below 278 K. The flow-tube became easily contaminated with yellow oily deposits on prolonged exposures which resulted in unusually large OH wall loss rates compared to that observed in a freshly coated flow-tube with the halocarbon wax. This was evident from the larger than normal intercepts in k versus $[(CH_3)_2NNH_2]$ plots even at the lowest $[OH]_o$ used. The flow-tube was frequently re-waxed to minimize this problem.

The slight negative temperature dependence and lack of pressure effect on k_1 suggests that the mechanism of OH attack involves its initial addition to N_2H_4 followed by fast

dissociation of the adduct to products (H_2O and N_2H_3). The findings of a previous ab-initio study by Armstrong et al. [3] on this reaction are qualitatively consistent with the present experimental observations. The shape of the potential energy profile along the reaction coordinate leading to N_2H_3 + H_2O as the products was examined. A single pre-reaction complex characterized by an OH---NN hydrogen-bond (OH---N distance 1.859Å, H---N-N angle 170.1°) was found at both B3LYP/6-31+G(D, P) and MP2/6-31+G(D, P) levels of theory. The G2(MP2) energy of this was computed to be ~ 5.5 kcal mol^{-1} lower than that of (N_2H_4 + OH). However, no transition-state for the direct H-abstraction by OH could be located at the B3LYP/6-31+G(D, P) level. Any approach by OH to an endo-H of hydrazine resulted in H-atom loss without activation. Instead, a transition-state structure for inversion of the N-atom bearing a hydrogen in close proximity to the hydroxyl was located at this level (N-H--OH angle 120.7°, NH--OH distance 1.707 Å, and NN-H distance 1.023 Å). The G2(MP2) energy of this transition-state was ~ 2.7 kcal mol^{-1} above that of the separated reactants. By contrast, at MP2/6-31+G(D, P) level, a well defined transition-state structure for H abstraction by OH was found (NN-H--OH angle 141.9°, NH--OH distance 1.459 Å, and NN-H distance 1.073 Å), its G2(MP2) energy being ~ 1.3 kcal mol^{-1} lower than that of the reactants. This transition-state was directly connected to the hydrogen-bonded pre-reaction complex. The MP2/6-31+G(D, P) description of the energetics of the reaction would predict a negative experimental activation energy and a pressure insensitive rate coefficient [**16**]. The results of the present gas phase work are consistent with this. In the future, it would be most interesting to see how the computed barrier to H-abstraction and vibrational frequency information on the transition-state and pre-reaction complex predict the absolute magnitude and temperature dependence of the OH + N_2H_4 gas phase reaction rate coefficient by means of transition-state theory rate expressions.

Despite increased complexity in the reaction mechanism from solvent/solute interactions in the liquid phase, the following comparisons can be made for the kinetics of the hydroxyl radical with hydrazine(s) where the same initial reaction products as those in the gas phase are formed. In basic aqueous solutions, Hayon and Simic [17] reported the room temperature rate coefficient to be 2.32 x 10^{-11} (±15%) cm^3 $molec^{-1}$ s^{-1} which was independent of pH in the range 9-11. This is comparable to the present gas phase value. However, more recently Buxton and Stuart **[18]** reported a smaller observed room temperature (293 K) reaction rate coefficient, k_{obs}, of (0.75 ± 0.08) x 10^{-11} cm^3 $molec^{-1}$ s^{-1} at pH = 11, which increased with temperature in the range 293-473 K in a non-Arrhenius fashion. At these high pHs, the hydroxyl radical interacts with neutral hydrazine that is preferentially hydrogen-bonds, via N-lone pair donation to the H-atom in water **[3,19]**, to form a solvent complex whose H-abstraction reaction with OH is partially diffusion controlled [17] to produce H_2O and the hydrazyl radical, N_2H_3. Buxton and Stuart modeled the non-Arrhenius behavior of k_{obs} by calculating the non-Arrhenius temperature dependence **[20,21]** of the diffusion controlled rate coefficient, $k_{diff} = (1/k_{obs} - 1/k_1)$, and interpolated a positive Arrhenius activation energy of ~ 2.6 Kcal mol^{-1} for k_1 in the aqueous solution. Existence of the hydrazyl radical in the liquid phase reaction was directly identified by the appearance/disappearance of a transient uv-absorption signal at λ_{max} = 230 nm at early (< ~ 50 μs) reaction times after the initiating radiolysis pulse. Furthermore, in acidic solutions, this prompt uv-absorption became much weaker with λ_{max} = ~ 225 nm which was identified to be due to the protonated hydrazyl, $N_2H_4^+$, formed from the reaction of OH with $N_2H_5^+$. A much smaller observed rate coefficient of (1.36 ± 0.08) x 10^{-13} cm^3 $molec^{-1}$ s^{-1} was measured at 293 K for pH values of 6 and below. Here, k_{obs} showed an upward curvature in the

Arrhenius plot, which could be rationalized by the fact that more free hydrazine became available ($N_2H_5^+ \Leftrightarrow N_2H_4 + H^+$) since the hydrozonium ion, $N_2H_5^+$, acid dissociation constant increased with temperature. In these experiments delayed transient uv-absorption at λ_{max} = ~ 230 nm was also seen at long (ms) reaction times after the initiating radiolysis pulse **[17,18,22]**. The kinetic behavior of which pointed to the triazene species, N_3H_3, formed in the unimolecular dissociation of the tetrazane, N_4H_6, intermediate as the source of the absorbance. The unobservable N_4H_6 species is directly formed in the self-reaction of the hydrazyl species, N_2H_3, formed in the initial OH attack on N_2H_4.

To our knowledge, such extensive product studies in the gas phase have not been carried out for OH plus di-amine systems, though in the related gas phase H-abstraction reaction, $H + N_2H_4 \rightarrow H_2 + N_2H_3$, the hydrazyl radical has been identified as a major product by its mass spectrum signal **[23,24]** and from stable end-product analyses **[25,26]**. N_2H_3 is also formed as a minor product in the gas phase reaction, $O + N_2H_4 \rightarrow$ products **[27,28]**. Our on previous work on unit H-atom primary quantum yield determinations in laser photolysis of di-amine vapors suggests that the corresponding stable co-fragment in the gas phase must be the hydrazyl radical **[4,6]**. Its gas phase ESR spectrum is known **[29]** and its low lying electronic structures have been computed previously **[30]**. The introduction of the CH_3 moiety in the hydrazine molecule opens up the possibility of direct H-abstraction from the stronger C-H bonds, or enhancement of hydrogen bonding tendency and eventual removal of the H-atom from the weaker N-H bond. On the other hand, fewer N-H sites (but more C-H sites) are present on increased methylation. Experimentally, we see an increase in the measured gas phase rate coefficient for CH_3NHNH_2

and $(CH_3)_2NNH_2$ compared to that for N_2H_4. Some empirical comparisons of the relative OH reactivity at the N-H center and the C-H site can be made. The per N-H reactivity of ~ 0.93 x 10^{-11} cm^3 s^{-1} in N_2H_4 if assumed to be the same in $(CH_3)_2NNH_2$ (i.e. the N-H site pre-exponential factor, A and the activation energy, E_A remain constant) would imply a reactivity of ~ 0.69 x 10^{-11} cm^3 s^{-1} for the C-H bond. Thus direct H-abstraction can compete with complex formation in $(CH_3)_2NNH_2$. Use of these reactivities in CH_3NHNH_2 together with the observed k_2 value at 298 K suggests a reactivity of ~ 2.18 x 10^{-11} cm^3 s^{-1} for the N-H with the methyl substitution, which is approximately twice that observed at the unsubstituted site. This enhancement could well be due to the formation of a more strongly bound hydrogen-bonded complex due to electron-donating effect of the methyl group compared to that formed at the unsubstituted site. Since in reality both the site-specific E_A and A values for a given reaction channel determine the overall reaction probability, only when absolute product yields and/or deuterium kinetic isotopic effects on the reaction rates are measured can we say which reaction path is the preferred mode for H-atom removal in OH plus di-amine system. It is encouraging to know that in the related amine homologous series: NH_3, NH_2CH_3, $NH(CH_3)_2$, $N(CH_3)_3$, the alkylated amine reactions with OH are also fast and show negative temperature dependencies **[31]**, while the ammonia reaction (involving H-atom metathesis) is slow and exhibits a positive temperature dependence **[32]**. It could well be that even here, methyl substitution promotes the formation of a hydrogen-bonded, $OH\text{---}NH_{(3-x)}(CH_3)_x$, pre-reaction complex (where x = 1,2,3) that dissociates quickly to eliminate H_2O and a radical co-fragment. The relative changes in the C-H and N-H bond energies in this homologous series **[33]** could well be influencing the site preference for H-atom removal to give the following observed reactivity trend of NH_2CH_3 <

$N(CH_3)_3 < NH(CH_3)_2$ **[31]**. For purely H-metathesis reactions of OH (and other radicals) with alkanes (and other reagents), strong correlations between C-H bond energy strength and measured reaction rates and/or product yields have amply been verified previously **[34]**.

The fate of di-amines in the atmosphere will be determined by their reactions with OH and O_3. Using an average value of ~ 1.1 x 10^6 molec cm^{-3} for the OH number density, lifetimes of ~ 6.6, ~ 4.1 and ~ 4.0 hours are calculated for N_2H_4, CH_3NHNH_2 and $(CH_3)_2NNH_2$, respectively for the troposphere at an average ambient temperature of 279 K. The corresponding lifetimes for reactions with ozone cannot be deduced accurately as only an upper limit for the O_3 + N_2H_4 reactivity is available in the literature. The rate coefficient is estimated to be ~ 1.4 x 10^{-16} cm^3 $molec^{-1}$ s^{-1} at 298 K **[35]**. Use of an ozone number density of 7.5 x 10^{11} molec cm^{-3} or less gives N_2H_4 lifetime of ~ 2.6 hours or longer. The lifetimes of the alkylated di-amines with respect to O_3 reaction may well be much shorter than this since they are thought to be much more reactive than N_2H_4 **[35]**. Therefore in urban air, during an ozone episode, the fate of the di-amines will most likely be governed by their degradation with ozone. An accurate assessment of the human health impact of the inherently toxic di-amines released at rocket launch sites must await proper determination of the O_3 reaction rates, and the elucidation of the subsequent degradation chemistry of the initial products which are also believed to be toxic and/or carcinogenic in nature.

ACKNOWLEDGMENT

Funding for this work was provided by the Air Force Office of Scientific Research under Contract # F04611-99-C-0025 with the Air Force Research Laboratory, Edwards AFB, CA 93524.

BIBLIORAPHY

1. Harris, G. W.; Atkinson, R.; Pitts, J. N. J Phys Chem 1979, **83**, 2557.
2. Hack, W.; Hoyermann, K.; Wagner, H. Gg. Ber Bunsenges Phys Chem 1976, **78**, 386.
3. Armstrong, D. A.; Yu, D.; Rauk, A. J Phys Chem A 1997, **101**, 4761.
4. Vaghjiani, G. L. J Phys Chem A 1997, **101**, 4167.
5. Vaghjiani, G. L. J Chem Phys 1996, **104**, 5479.
6. Vaghjiani, G. L. J Chem Phys1993, **98**, 2123.
7. Vaghjiani, G. L.; Ravishankara, A. R. J Phys Chem 1989, **93**, 1948.
8. Greenblatt, G. D.; Ravishankara, A. R. J Geophys Res 1990, **95**, 3539.
9. Wine, P. H.; Ravishankara, A. R. Chem Phys 1982, **69**, 365.
10. Streit, G. E.; Howard, C. J.; Schmeltekopf, A. L.; Davidson, J. A.; Schiff, H. I. J Chem Phys 1976, **65**, 4761.
11. G. A.; Jeffries, J. B.; Rensberger, K. J.; Crosley, D. R. J Chem Phys 1990, **92**, 7258.
12. Vaghjiani, G. L. J Chem Phys 2000, **to be submitted**.
13. Howard, C. J. J Phys Chem 1979, **83**, 3.
14. Kaufman, F. Proc R Soc London Ser A 1958, **247**, 123 and Prog React Kinet 1961, **1**, 3.

15. Hirschfelder, J. D.; Curtiss, C. F.; Bird, R. B. *Molecular Theory of Gases and Liquids;* Wiley Publ.: New York, 1954.

16. See for example: Chen, Y.; Rauk, A.; Roux, E. T. J Phys Chem 1991, **95**, 9900 and Berry, R. J.; Marshall, P. Int J Chem Kinet 1998, **30**, 179.

17. Hayon, E.; Simic, M. J Am Chem Soc 1972, **94**, 42.

18. Buxton, G. V.; Stuart, C. R. J Chem Soc Faraday Trans 1996, **92**, 1519.

19. Yu, D.; Rauk, A.; Armstrong, A. Can J Chem 1994, **72**, 471.

20. Smoluchowski, von M. Z Phys Chem 1917, **92**, 129.

21. Elliot, A. J.; McCracken, D. R.; Buxton, G. V.; Wood, N. D. J Chem Soc Faraday Trans I 1990, **86**, 1539

22. Southland, J. W. J Phys Chem 1979, **83**, 789.

23. Gehring, M.; Hoyermann, K.; Wagner, H. Gg.; Wolfrum, J. Ber Bunsenges Phys Chem 1971, **75**, 1287.

24. Foner, S. N.; Hudson, R. L. J Chem Phys 1958, **29**, 442 and 1970, **53**, 4377.

25. Schiavello, M.; Volpi, G.G. J Chem Phys 1963, **37**, 1510.

26. Stief, L. J.; DeCarlo, V.J.; Mataloni, R. J. J Chem Phys 1967, **46**, 592.

27. Foner, S. N.; Hudson, R. L. J Chem Phys 1968, **49**, 3724.

28. Gehring, von M.; Hoyermann, K.; Wagner, H. Gg.; Wolfrum, J. Ber Bunsenges Phys Chem 1969, **73**, 956 and Gehring, M.; Hoyermann, K.; Schacke, H.; Wolfrum, J. Symp (Int) Combust Proc 1972, **14**, 99.

29. Fantechi, R.; Helcke, G. A. J Chem Soc Faraday Trans II 1972, **68**, 924.

30. Chandler, G. S.; McLean, A. D. J Chem Phys 1979, **71**, 2175.

31. Atkinson, R.; Perry, R. A.; Pitts, J. N. Jr. J Chem Phys 1978, **68**, 1850 and 1977, **66**, 1578.

32. See for example: Diau, E. W. -G.; Tso, T. -L.; Lee, Y. -P. J Phys Chem 1990, **94**, 5261 and Smith, I. W. M.; Zellner, R. Int J Chem Kinet 1975, **1**, 341.

33. McMillen, D. F.; Golden, D. M. Ann Rev Phys Chem 1982, **33**, 493 and references therein.

34. See for example: Tully, F. P. Chem Phys Lett 1988, **143**, 510, Hess, E. P.; Durant, J. L. Jr.; Tully, F. P. J Phys Chem 1989, **93**, 6402 and Atkinson, R. J Phys Chem Ref Data 1989, Monograph 1 and references therein.

35. Tuazon, E. C.; Carter, W. P. L.; Winer, A. M.; Pitts, J. N. Jr. Environ Sci Technol 1981, **15**, 823.

Table I Temperature dependence of OH + N_2H_4 reaction rate coefficient, k_1.

T(K)	[a]k_1(10^{-13} cm^3 $molec^{-1}$ s^{-1})	[b]Pressure (torr)	OH-Source	[c]$[OH]_o$(10^{10} cm^{-3})	v (cm s^{-1})
232.0	475.0	1.84	H_2-discharge/NO_2-titration side-arm port[f]	18.0	1961
255.0	440.8	1.84	H_2-discharge/NO_2-titration sliding-injector	9.52	2270
255.0	454.0	1.86	H_2-discharge/NO_2-titration side-arm port[f]	11.0	2112
278.0	322.0	1.85	H_2-discharge/NO_2-titration sliding-injector	14.9	2251
278.0	353.4	1.84	H_2-discharge/NO_2-titration sliding-injector	8.74	2474
279.0	380.3	1.86	CF_4-discharge/H_2O-titration side-arm port	1.72	2345
292.0	386.1	1.84	H_2-discharge/NO_2-titration sliding-injector	8.32	2587
298.0	361.0	1.87	CF_4-discharge/H_2O-titration side-arm port	1.55	2468
298.0	363.0	1.76	H_2-discharge/NO_2-titration sliding-injector	10.8	2572
2980	383.0	1.77	H_2-discharge/NO_2-titration sliding-injector	11.6	2518
298.0	362.2	1.81[d]	O_2-discharge, sliding-injector look at OH appearance	19.1 ($[O]_o$)	2556
298.0	398.0	1.78	H_2-discharge/NO_2-titration sliding-injector	0.50	2536
299.0	391.0	1.82	CF_4-discharge/H_2O-titration side-arm port	6.99	2488
324.0	338.0	1.84	H_2-discharge/NO_2-titration sliding-injector	7.50	2810
374.0	268.3	1.83	H_2-discharge/NO_2-titration sliding-injector	6.50	3235
290.0	393.7	441.4	N_2O/H_2O-photolysis 3 Hz 193-nm laser rap rate	80.5	7.83
290.0	403.3	441.4	N_2O/H_2O-photolysis 3 Hz 193-nm laser rap rate	12.6	7.83
290.0	378.5	52.01	N_2O/H_2O-photolysis 3 Hz 193-nm laser rap rate	43.8	17.41
291.0	321.2	403.2 (N_2)[e]	N_2O/N_2-photolysis 2 Hz 193-nm laser rap rate look at OH appearance	76.0 ($[O]_o$)	14.63
295.0	390.8	21.31 (N_2)[e]	N_2O/N_2-photolysis 3 Hz 193-nm laser rap rate look at OH appearance	56.0 ($[O]_o$)	44.76
295.0	381.0	186.3 (N_2)[e]	N_2O/N_2-photolysis 3 Hz 193-nm laser rap rate look at OH appearance	59.0 ($[O]_o$)	10.63
359.0	337.0	51.85	N_2O/H_2O-photolysis 3 Hz 193-nm laser rap rate	35.3	21.62
491.0	316.7	50.92	N_2O/H_2O-photolysis 3 Hz 193-nm laser rap rate	25.8	29.98

Table I continued;

T(K)	[a]k_1(10^{-13} cm^3 $molec^{-1}$ s^{-1})	[b]Pressure (torr)	OH-Source	[c]$[OH]_o$(10^{10} cm^{-3})	v (cm s^{-1})
628.0	303.1	51.25	N_2O/H_2O-photolysis 3 Hz 193-nm laser rap rate	16.3	38.88
633.0	292.9	51.25	N_2O/H_2O-photolysis 3 Hz 193-nm laser rap rate	11.3	38.98

[a]Overall 1-σ uncertainty in k_1 is ~ ± 18% (precision plus estimated systematic).

[b]Pressure of He carrier gas unless otherwise stated.

[c]When O-atoms are reacted with N_2H_4, the initial O-atom concentration, $[O]_o$ is indicated.

[d]Excess $[H_2O]$ (1.0×10^{15} molec cm^{-3}) present.

[e]Excess $[CO_2]$ (8.1×10^{16} molec cm^{-3}) present.

[f]OH-fluorescence signal decay recorded for a fixed injector position, z and varying $[N_2H_4]$. The observed 1^{st}-order decays at each position are then plotted as a function of z to calculate k_1. This approach at low-T gave somewhat better reproducibility in the measured decay rate compared to that when the decay rate was measured for a fixed $[N_2H_4]$ and varying z.

Table II Temperature dependence of OH + CH_3NHNH_2 reaction rate coefficient, k_2.

T(K)	$a_{k_2}(10^{-13}$ cm^3 molec^{-1} s$^{-1})$	He Pressure (torr)	OH-Source	$[OH]_o(10^{10}$ cm$^{-3})$	v (cm s^{-1})
258.0	645.1	2.00	H_2-discharge/NO_2-titration side-arm port	2.63	2803
278.0	637.1	2.06	H_2-discharge/NO_2-titration side-arm port	1.48	2983
292.0	565.0	2.09	H_2-discharge/NO_2-titration side-arm port	4.40	3209
298.0	561.0	1.9.0	H_2-discharge/NO_2-titration sliding-injector	2.50	3300
298.0	613.0	1.97	H_2-discharge/NO_2-titration sliding-injector	0.76	3096
298.0	564.4	2.02	H_2-discharge/NO_2-titration side-arm port	1.17	3225
298.0	640.0	2.02	H_2-discharge/NO_2-titration side-arm port	2.15	3203
316.0	540.0	2.06	H_2-discharge/NO_2-titration side-arm port	2.12	3374
345.0	506.8	2.11	H_2-discharge/NO_2-titration side-arm port	2.91	3685
373.0	528.1	2.08	H_2-discharge/NO_2-titration side-arm port	2.73	4023
289.0	691.3	51.05	N_2O/H_2O-photolysis 3 Hz 193-nm laser rap rate	33.6	17.08
289.0	697.5	50.98	N_2O/H_2O-photolysis 3 Hz 193-nm laser rap rate	1.98	17.53
289.0	604.8	503.7	N_2O/H_2O-photolysis 3 Hz 193-nm laser rap rate	76.2	6.44
357.0	648.3	51.78	N_2O/H_2O-photolysis 3 Hz 193-nm laser rap rate	29.2	21.32
475.0	588.4	51.55	N_2O/H_2O-photolysis 3 Hz 193-nm laser rap rate	21.9	28.50
637.0	529.1	487.9	N_2O/H_2O-photolysis 2 Hz 193-nm laser rap rate	34.1	14.11

[a]Overall 1-σ uncertainty in k_2 is ~ $\pm$ 18% (precision plus estimated systematic).

Table III Temperature dependence of OH + $(CH_3)_2NNH_2$ reaction rate coefficient, k_3.

T(K)	[a]k_1(10^{-13} cm^3 $molec^{-1}$ s^{-1})	He Pressure (torr)	OH-Source	$[OH]_o$(10^{10} cm^{-3})	v ($cm\ s^{-1}$)
254.0	724.5	1.99	H_2-discharge/NO_2-titration side-arm port	2.85	2834
278.0	745.5	2.04	H_2-discharge/NO_2-titration side-arm port	1.93	3034
296.0	576.9	2.01	H_2-discharge/NO_2-titration side-arm port	1.04	3387
297.0	573.1	2.05	H_2-discharge/NO_2-titration side-arm port	1.18	3216
298.0	641.0	1.98	H_2-discharge/NO_2-titration side-arm port	3.20	3368
298.0	534.0	2.06	H_2-discharge/NO_2-titration side-arm port	1.10	3124
298.0	606.8	1.97	H_2-discharge/NO_2-titration sliding-injector	1.20	2956
298.0	635.6	1.94	H_2-discharge/NO_2-titration sliding-injector	1.57	3158
298.0	693.0	2.16	H_2-discharge/NO_2-titration sliding-injector	1.61	3012
315.0	560.4	2.01	H_2-discharge/NO_2-titration side-arm port	3.05	3507
341.0	535.0	2.02	H_2-discharge/NO_2-titration side-arm port	2.83	3790
373.0	498.0	2.06	H_2-discharge/NO_2-titration side-arm port	1.85	3991
296.0	572.0	36.2	N_2O/H_2O-photolysis 10 Hz 193-nm laser rap rate	196.0	20.10
297.0	570.0	35.1	N_2O/H_2O-photolysis 10 Hz 193-nm laser rap rate	86.1	20.30
446.0	472.6	32.6	N_2O/H_2O-photolysis 10 Hz 193-nm laser rap rate	108.7	34.10
533.0	447.4	33.4	N_2O/H_2O-photolysis 10 Hz 193-nm laser rap rate	185.7	39.98
630.0	499.1	33.4	N_2O/H_2O-photolysis 10 Hz 193-nm laser rap rate	3.52	48.60
630.0	472.3	33.4	N_2O/H_2O-photolysis 10 Hz 193-nm laser rap rate	150.5	48.60
632.0	476.0	530.0	N_2O/H_2O-photolysis 1 Hz 193-nm laser rap rate	155.2	13.43
632.0	376.0	530.0	N_2O/H_2O-photolysis 10 Hz 193-nm laser rap rate	155.2	13.43
633.0	475.9	508.0	N_2O/H_2O-photolysis 2 Hz 193-nm laser rap rate	34.1	13.79

[a]Overall 1-σ uncertainty in k_3 is ~ $\pm$ 18% (precision plus estimated systematic).

FIGURE CAPTIONS

Figure 1 Measured OH-fluorescence signal, OH_S as a function of flow-tube reaction time, t in different $(CH_3)_2NNH_2$ concentrations; = zero (crosses), = 0.292×10^{13} (open circles), = 0.643×10^{13} (open triangles), = 0.957×10^{13} (open squares), and = 1.339×10^{13} molec cm^{-3} (open diamonds) at 373 K and in 2 torr He. OH is produced in the side-arm discharge port.

Figure 2 Plot of pseudo-first-order decay coefficients, $k_{net} = (k + k_{W,i})$ versus the $[(CH_3)_2NNH_2]$ of Figure 1. Because the upward correction, Refs. [13,14], of k_{net} for axial diffusion, $k_{corr} = k_{net}(1 + k_{net}\mathcal{D}/v^2)$, where $\mathcal{D}$, in units of $cm^2\ s^{-1}$, is the diffusion coefficient of OH in He is expected to be < 5%, Ref. [15], the flow-tube data was not corrected for this since the other overall errors in the experiment are calculated to be ~ ± 18%, Ref. [5]. The absolute second-order rate coefficient, k_3 is determined to be $(4.98 \pm 0.89) \times 10^{-11}$ cm^3 $molec^{-1}$ s^{-1} at 373 K.

Figure 3 OH appearance profile in the O + N_2H_4 reaction during 193-nm photolysis of N_2O (2.1×10^{15}) in N_2 (6.2×10^{17}) and CO_2 (8.1×10^{16} molec cm^{-3}). The laser fluence was ~ 1.6 mJ/cm^2/pulse and N_2H_4 concentration was 1.10×10^{13} molec cm^{-3}. The characteristic coefficients of appearance and decay in the signal yield values for k_1(phenomenological) and k_O, respectively. Where k_O is the absolute second-order rate coefficient for O-atom reaction with hydrazine, and k_1(phenomenological) corresponds closely to the absolute second-order rate coefficient for OH reaction with the di-amine.

Figure 4 The Arrhenius temperature dependencies of the absolute second-order rate coefficients; k_1, k_2 and k_3 for OH reactions with N_2H_4 (diamonds), CH_3NHNH_2 (circles), and $(CH_3)_2NNH_2$ (squares), respectively. Open data points were obtained using the flow-tube apparatus and solid data points using the pulsed-photolysis reactor. Previous results of Ref. [1] (crosses) and Ref. [2] (plus) are also shown.

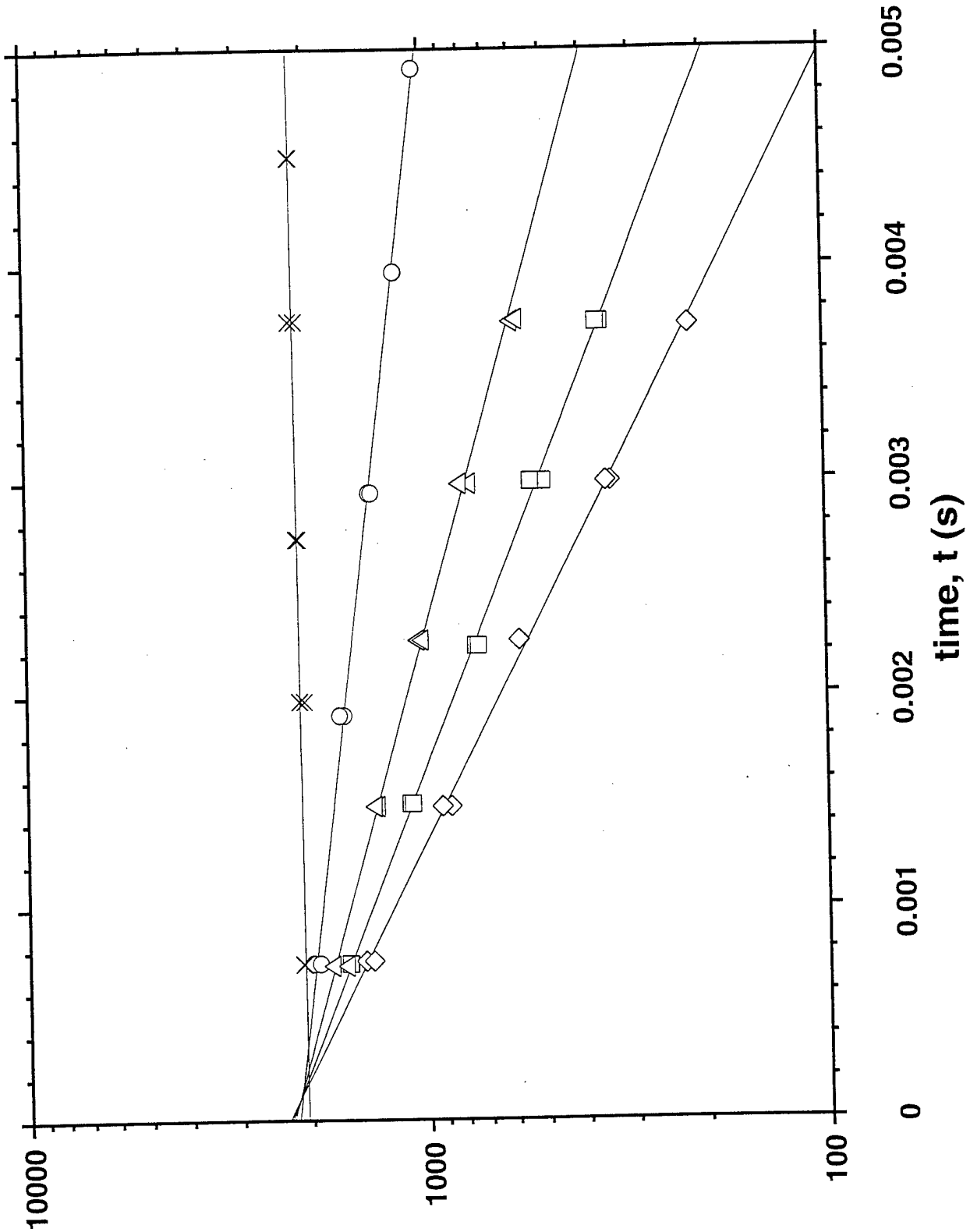
10000
1000
100
0
0.001
0.002
0.003
0.004
0.005
time, t (s)
S_{HO} (arbitrary units)

Figure 1

Figure 2

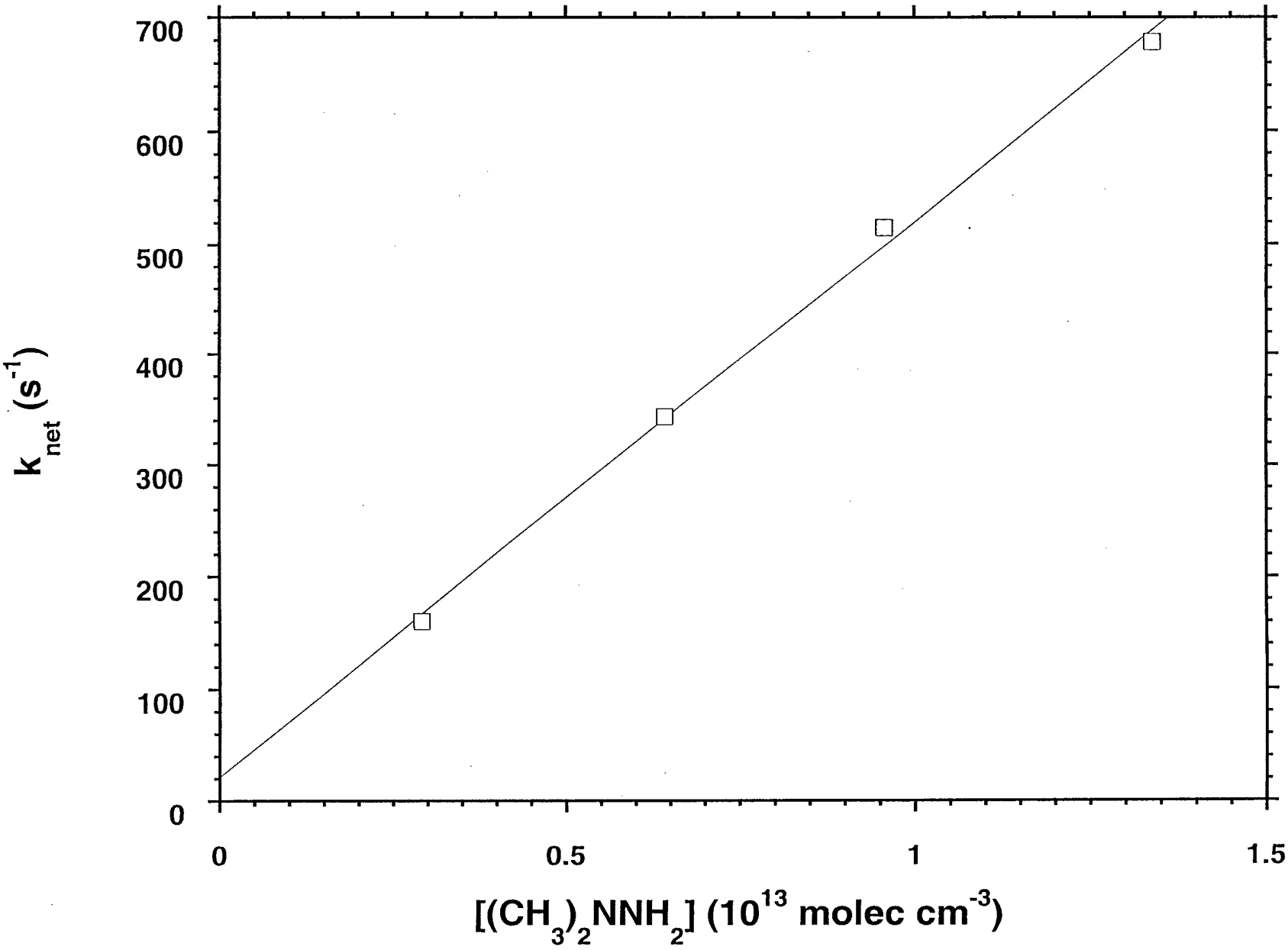
700
600
500
400
300
200
100
0
0
0.5
1
1.5
k_{net} (s^{-1})
$[(CH_3)_2NNH_2]$ (10^{13} molec cm^{-3})

Figure 3

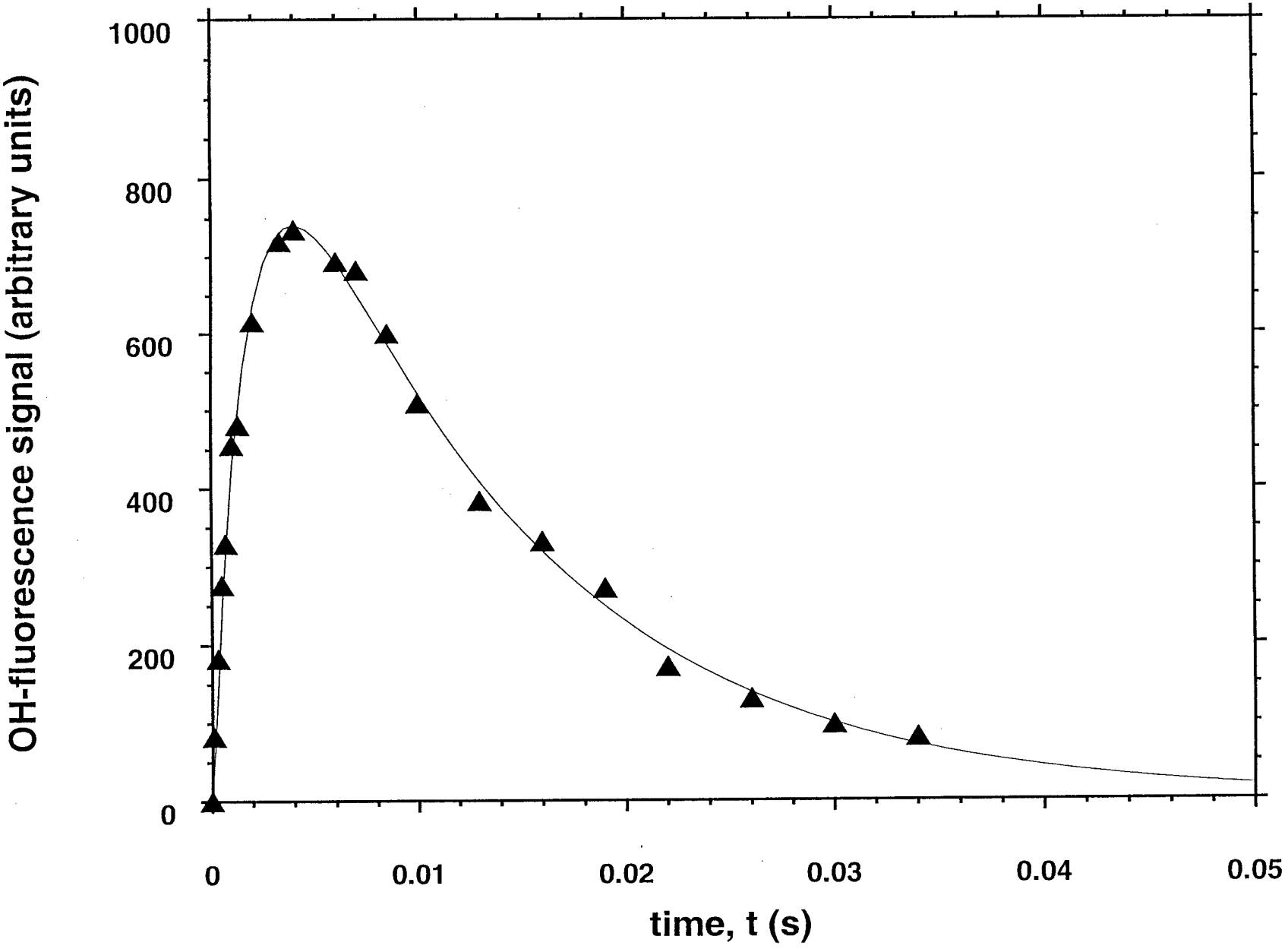
OH-fluorescence signal (arbitrary units)
1000
800
600
400
200
0
0
0.01
0.02
0.03
0.04
0.05
time, t (s)

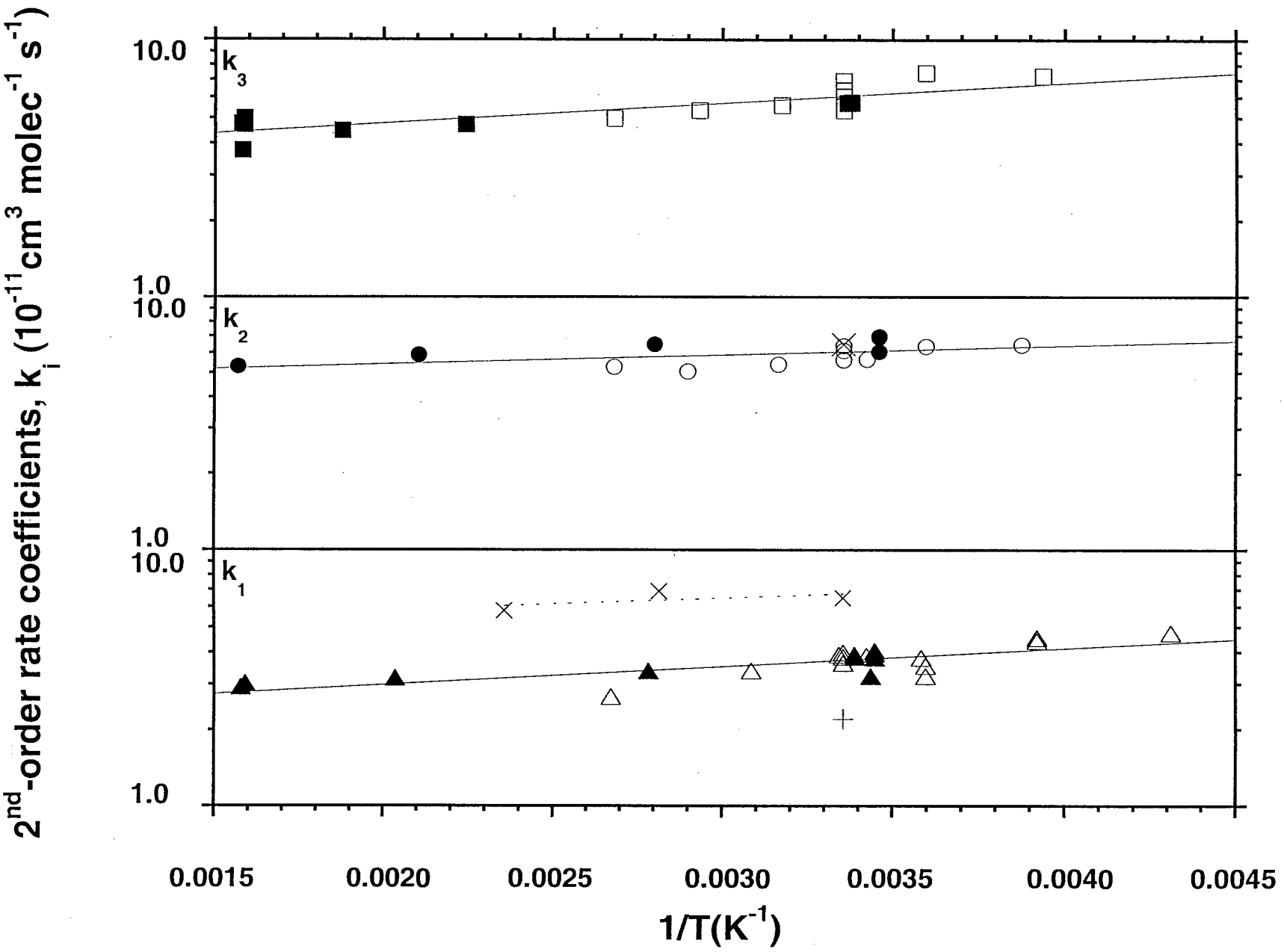
10.0
k3
1.0
10.0
k2
1.0
10.0
k1
1.0
2nd-order rate coefficients, ki (10-11cm3 molec-1 s-1)
0.0015
0.0020
0.0025
0.0030
0.0035
0.0040
0.0045
1/T(K-1)